Oxidation Kinetics of Mg-, Si-, and Fe-Implanted Aluminum by Using X-ray Photoelectron Spectroscopy

T. Do[†,‡] and N. S. McIntyre[‡,§]

Department of Materials and Mechanical Engineering, University of Western Ontario, London, Ontario, Canada N6A 5B9; Surface Science Western, University of Western Ontario, London, Ontario, Canada N6A 5B7; and Department of Chemistry, University of Western Ontario, London, Ontario, Canada N6A 5B7

P. A. W. van der Heide

Department of Chemistry, University of Houston, Houston, Texas 77204-5641

U. G. Akano

Department of Physics, University of Western Ontario, London, Ontario, Canada N6A 3K7

Received: July 29, 1998; In Final Form: December 16, 1998

The oxidation kinetics of Mg-, Si-, and Fe-implanted aluminum has been studied at room temperature and a water vapor pressure of 2.0×10^{-6} Pa using X-ray photoelectron spectroscopy. The elements Mg, Si, and Fe were implanted into high-purity aluminum at low ion doses from 6.0×10^{12} to 3.6×10^{13} ions·cm^{-2}. Secondary ion mass spectrometry (SIMS) depth profiles have shown that the element distributions of Mg and Fe in aluminum are consistent with the theoretical depth profiles calculated using a TRIM (transport of ions in matter) program. The implanted elements are distributed in the near-surface region with their maximum concentration at the depth of ∼50 nm. In the case of implanted Si, however, SIMS depth profile shows no maximum concentration peak and the near-surface concentration is much higher than that calculated. This is ascribed to diffusion of Si toward the surface during implantation. Oxidation kinetics of implanted aluminum have shown that surface concentrations of implanted Si, as low as 40 ppm, cause an increase in the Al oxidation rate compared to the pure metal. By contrast, implanted Mg, surface concentration from 20 to 120 ppm, results in a lowered oxidation rate until the oxide reaches a thickness of ∼0.55 nm, and after that a rapid increase in oxidation occurs. Implanted Fe does not cause any change in the oxidation rate of aluminum. These oxidation kinetics can be explained on the basis of metal vacancies in the defect structure of aluminum thin oxide films. The effects of surface damage caused by the ion beam during the implantation experiment were also determined by measurements of oxidation kinetics.

1. Introduction

It is well-known that the type and concentration of impurities can modify significantly the defect structure of an oxide[1] and, as a result, may change the mechanism of transport of matter through the oxide layers and the related oxidation kinetics. The direction and order of changes in oxidation kinetics depend on the type and concentration of defects in the host oxide structure, which in turn, determine the type and concentration level of an impurity that might effectively change the transport properties. This work describes the changes in oxidation rate of aluminum in the presence of elemental "impurities" doped into metal surface using ion implantation prior to oxidation. This is a particularly useful approach in the case of thin oxide films with a very low defect concentration, which require equivalent concentration of the impurity element in order to observe any change in transport properties that may result from its presence in the oxide layer.

In the case of the thin film of oxide, which forms on aluminum at ambient conditions, the defect structure is rather complicated and not well established. There are difficulties in studying the oxidation process of aluminum caused by a low oxidation rate and a very thin oxide overlayer, suggesting extremely low defect concentration in the oxide structure, which require the use of sophisticated analytical and experimental techniques. In normal conditions the interaction of clean aluminum surfaces with oxygen or water vapor results in a thin amorphous oxide overlayer, which tends to crystallize into γ-Al_2O_3 with further thermal treatment above 450 °C.[2−4] On the other hand, the γ-Al_2O_3 phase, known as a product of the dehydration of boehmite or of anodic oxidation, has a defective spinel structure, in which the oxygen lattice is well ordered but the tetrahedral Al lattice is strongly disordered.[5,6] Although a number of studies exist on interaction of aluminum with oxygen and water vapor,[7−13] the nature of thin aluminum oxide films still remains largely unknown.

The initial interaction of water vapor with pure polycrystalline aluminum surfaces has previously been examined in detail in this laboratory.[14] Using Auger electron spectroscopy (AES) and X-ray photoelectron spectroscopy (XPS), the oxidation kinetics of aluminum in room temperature was followed from sub-

* Corresponding author. Fax: +1 (519) 661 3709. E-mail: thando@surf.ssw.uwo.ca.
† Department of Materials and Mechanical Engineering.
‡ Surface Science Western.
§ Department of Chemistry.

10.1021/jp983221o CCC: $18.00
Published on Web 03/12/1999

TABLE 1: Major Impurities in the Pure Aluminum Samples Determined by Spark Source Mass Spectrometry (in Particles per million (ppm))[a]

element	As	Bi	Ca	Cr	Cu	Fe	K
concn (ppm)	<0.05	0.02	0.3	≤0.04	0.2	0.2	0.3
element	Li	Mg	Mn	Na	Ni	Si	Zn
concn (ppm)	<0.1	1	≤0.04	0.2	≤0.1	1	≤0.2

[a] All other metallic elements are below detection limit, which is 0.1 ppm.

Langmuir to mega-Langmuir levels of water vapor exposure. The relationship between the oxidation kinetics of pure aluminum and the pressures of water vapor suggested that the cation vacancies may be the major point defects that are involved in determining the rate process in the growth of thin oxide films.[15] In the present work, the oxidation kinetics of aluminum are shown to be affected by impurity elements such as Mg and Si but not Fe, all of which were introduced into pure aluminum by ion implantation at near-surface concentrations as low as 20−160 ppm. These effects can be explained on the basis of dominating metal vacancies in the defect structure of the aluminum thin oxide films.

2. Experimental Section

Polycrystalline aluminum (99.999% purity) used in this work was supplied by Alcan International Ltd., Kingston, Ontario. Specimens were polished to a 0.05 μm Al_2O_3 finish, degreased ultrasonically, and annealed in a vacuum at 300 °C for 30 min. Such prepared samples were implanted with the elements Mg, Si, and Fe with a beam energy of 40 keV and low ion doses from 6.0×10^{12} to 3.6×10^{13} ions·cm^{-2}. The implantation was performed on a Tandetron accelerator in the Department of Physics, The University of Western Ontario. The ion dose and beam energy were designed by calculations using the TRIM (transport of ions in matter)[16,17] program to give concentrations of the implanted element in the near-surface region of a few tens of ppm and the maximum of the implanted profile at the depth of ∼50 nm. This program makes use of the Monte Carlo method to simulate the slowing down and scattering of energetic ions, which can be any element in the periodic table, in metals and various solid compounds. Because of its consistency with experimental results, the TRIM program is widely used in ion implantation to estimate the ion range and damage distributions as well as energy distributions of backscattered and transmitted ions. The program is very simple to use and easily accessible;[17] therefore, for a clear presentation of our experimental results, the results of all TRIM calculations are not showed here. For comparison, Table 1 shows the major impurities (in ppm) in high-purity aluminum samples used throughout this work. No postimplantation annealing stage was performed in order to avoid the possible segregation of implanted elements to the surface or to grain boundaries.

Because of the native oxide present, before exposure to water vapor, the surfaces of implanted samples were cleaned in situ by Ar^+ ion bombardment (3 keV, 10 min) with the incident angle 55° off the surface normal and an ion dose at $\sim 3 \times 10^{14}$ ions·cm^{-2}; this is the minimum Ar^+ ions dose estimated to produce satisfactorily clean aluminum surfaces; the cleanness was confirmed by the absence of an oxygen O(1s) peak in a high-resolution XPS spectrum. Clean aluminum surfaces were then exposed to water vapor in a separate custom-designed preparation chamber attached to the XPS spectrometer at a pressure of 2.0×10^{-6} Pa and for exposure time from 1 to 60 min. After exposure to water vapor, the implanted samples were transferred back into the XPS analytical chamber and an XPS spectrum was taken at an operating base pressure of 4.0×10^{-7} Pa. All spectra were obtained using a Surface Science Laboratories SSX-100 spectrometer equipped with a monochromatic Al Kα (1486.6 eV) X-ray source. The binding energy scale was calibrated to give an Au $4f_{7/2}$ line position of 83.98 eV for metallic gold. The pass energy of the hemispherical analyzer was maintained at 50 eV, giving a constant energy resolution of 0.53 eV. The intensity of a photoelectron peak was measured by calculation of the area under the peak using a least-squares fitting routine developed by Surface Science Laboratories, Inc. After a Shirley correction was made to the background,[18] all peaks were fitted with a 70% Gaussian shape (and 30% Lorentzian) for the metallic peak and a 100% Gaussian shape for the oxidic peaks. The uptake of oxygen on clean surfaces of implanted aluminum samples, at room temperature, was monitored by following the changes in the intensity of XPS Al(2p) and O(1s) photoelectron lines.

Secondary ion mass spectrometry (SIMS) was used to examine the spatial distribution of implanted elements in the specimens. Both 3D and normal depth profiles were employed. In both cases SIMS analyses were obtained using a Cameca IMS-3f instrument, which was operated with an O_2^+ primary ion beam, and current of 250 nA at 2 kV energy, rastered over a 250 × 250 μm^2 area. The primary beam O_2^+ was chosen because of its enhancement in the ion yields for these elements used as implants, and because of its relatively low sputter rate. The method of collection of 3D SIMS profiles has been described in detail elsewhere.[19−21] The SIMS depth profiles were performed for all implanted samples, both in the as-received condition and after surface cleaning by Ar^+ ion bombardment in the XPS instrument prior to exposure to water vapor. While the former provided the depth profile of the implanted element, the latter was intended to determine its actual concentration in near-surface area of clean surfaces at the moment of exposure experiment. The concentrations of an implanted element in the SIMS depth profiles are calculated based on the relative ratios of ion intensities to its background intensity, which corresponds to the impurity level given in Table 1. For samples cleaned by Ar^+ ion bombardment it has been estimated that, on average, a top layer about average thickness of 20 nm was removed after the surface cleaning procedure.

3. Results and Discussion

Figure 1 shows the representative 3D imaging depth profiles for the ions $^{24}Mg^+$, $^{28}Si^+$, and $^{56}Fe^+$ of three implanted aluminum samples, with the maximum dose of implant used in for each element. Each cylinder consisted of several "image-slices" showing the lateral distribution of the implanted element within the same block of the sample; with the total depth (height of the cylinder) indicated on Figure 1. The top of each cylinder represents the first acquired image of the implanted element distribution; the aluminum matrix is the black background, and the brightness determines the intensity of the implanted element. The imaging $^{28}Si^+$ and $^{56}Fe^+$ depth profiles show the highest intensities at the outermost layer; by contrast, the $^{24}Mg^+$ ions show maximum intensity in the near-surface layers. These image depth profiles show no evidence of precipitation of implanted elements in aluminum.

Figures 2, 3, and 4 represent the SIMS depth profiles of implanted element in Fe-, Mg-, and Si-implanted aluminum

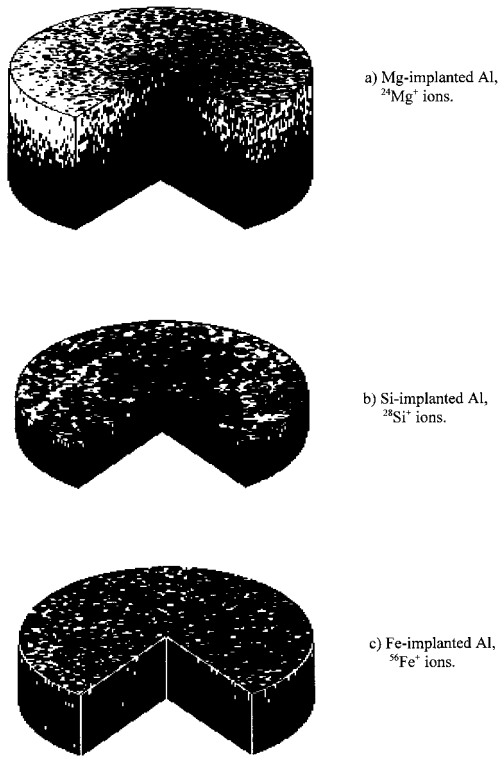

Figure 1. Three-dimensional SIMS imaging depth profiles of the implanted element in (a) Mg-implanted, (b) Si-implanted, and (c) Fe-implanted aluminum samples with implant dose of (a) 3.6×10^{13} atoms·cm^{-2}, (b) 4.0×10^{13} atoms·cm^{-2}, and (c) 3.0×10^{13} atoms·cm^{-2}, respectively. The diameter of the cylinders is 150 μm and their depth is approximately (a) 0.5 μm, (b) 0.1 μm, and (c) 0.3 μm.

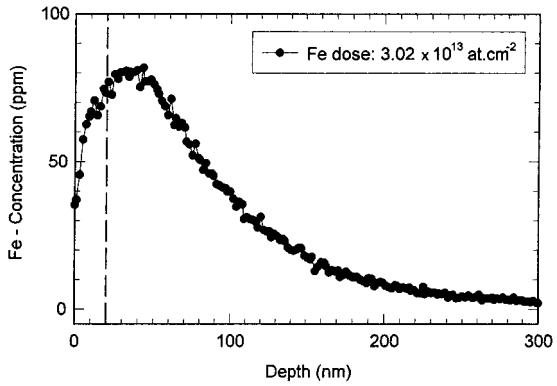

Figure 2. SIMS depth profile of the Fe-implanted aluminum samples. The vertical dashed line indicates the level of concentrations of the implanted Fe on aluminum surfaces after cleaning procedure.

samples with different doses of the implant. The dashed vertical lines at a depth of 20 nm in each figure show the average implant concentration at near-surface after surface cleaning by 3 keV Ar^+ ions sputtering, i.e., implant concentration on clean aluminum surfaces prior to exposing to water vapor. From Figures 2 and 3, the depth profiles of the implanted elements Fe and Mg show typical bell-shaped implant distributions. These distributions are consistent with those calculated using the TRIM program for 40 keV ions of Fe and Mg bombarded vertically into the Al target. After Ar^+ bombardment, the concentration of implanted Fe and Mg on clean aluminum surfaces are respectively 80 ppm (Fe dose of 3.02×10^{13} atoms·cm^{-2}), and 20, 40, and 120 ppm (Mg-implanted, doses of 0.6×10^{13}, 1.21×10^{13}, and 3.63×10^{13} atoms·cm^{-2}). By contrast, an unusual distribution of implanted Si were observed by SIMS depth profiles for all doses (see Figure 4). These depth profiles have

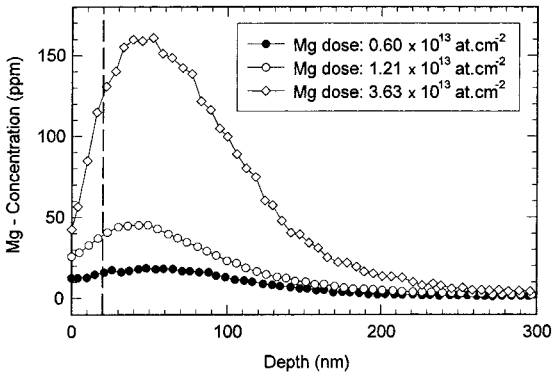

Figure 3. SIMS depth profiles of the Mg-implanted aluminum samples for the three different doses. The vertical dashed line indicates the level of concentrations of the implanted Mg on aluminum surfaces after cleaning procedure.

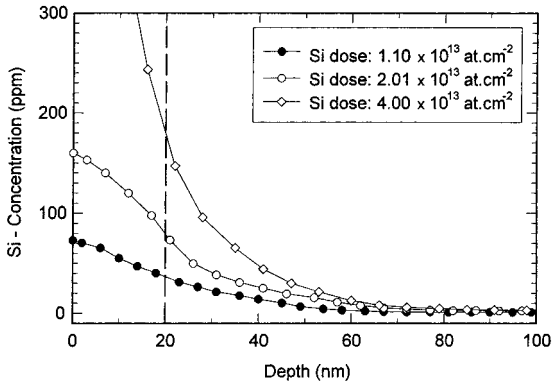

Figure 4. SIMS depth profiles of the Si-implanted aluminum samples for the three indicated doses. The vertical dashed line indicates the level of concentrations of the implanted Si on aluminum surfaces after cleaning procedure.

no maximum concentration peak compared with those calculated using the TRIM program for 40 keV Si ions incident vertically into the Al target. Instead, the highest Si concentration was detected at a near-surface layer, suggesting a strong diffusion of Si toward the aluminum surface during the implantation process. However, this is a very complex phenomenon, which can be affected by various factors such as incident beam energy, ion dose during ion implantation, and substrate surface texture; further studies are continuing in this laboratory to explain the observed effects. The average Si concentrations on the aluminum surfaces during the H_2O exposure experiment were 40, 80, and 160 ppm for implant doses of 1.10×10^{13}, 2.01×10^{13}, and 4.0×10^{13} atoms·cm^{-2}, respectively (see the dashed line in Figure 4).

Exposing the clean aluminum surfaces to water vapor results in a growth of oxide layers, which cause not only an attenuation of the photoelectron intensity originating from the metal substrate but also a shift in binding energy of the photoelectron from metallic atoms in the oxide overlayer due to its new chemical environment; the latter develops as a new photoelectron line assigned to an oxidic component. Thus, increasing the exposure time results in a decrease of intensity of the Al(2p) metallic, binding energy at 72.87 eV, an increase of the Al(2p) oxidic component, binding energy at 75.80 eV, and a simultaneous increase of intensity of the O(1s) photoelectron line with a binding energy at 532.30 eV. The intensity ratios between the oxidic and the metallic components in the XPS Al(2p) spectrum, I_o/I_m, is then a measure of the growth of the oxide layers and can be used to calculated its thickness d using the

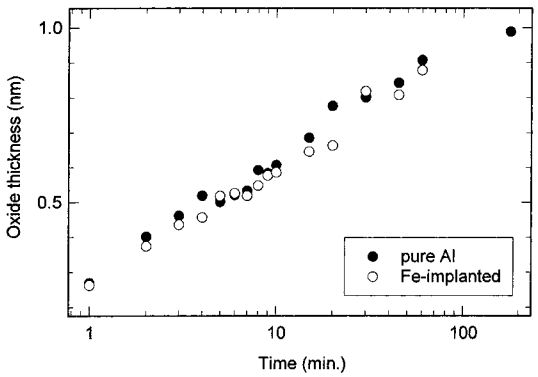

Figure 5. A comparison between oxidation kinetics of Fe-implanted and pure aluminum.

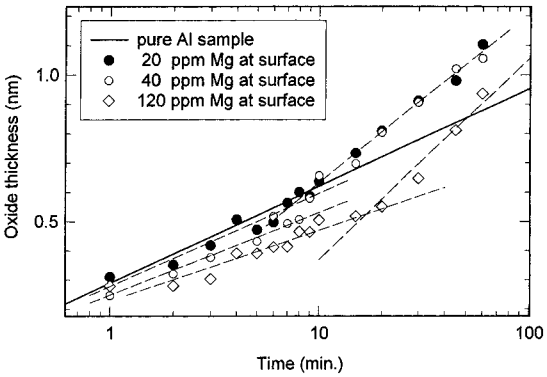

Figure 6. Oxidation kinetics of Mg-implanted aluminum. The concentrations of implanted Mg on clean aluminum surfaces before exposure to water vapor are as indicated on the SIMS depth profiles, Figure 3.

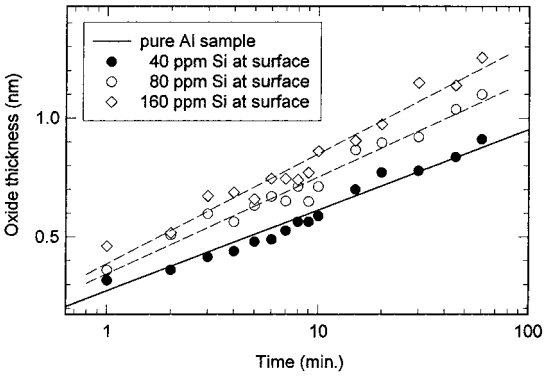

Figure 7. Oxidation kinetics of Si-implanted aluminum. The concentrations of implanted Si on clean aluminum surfaces before exposure to water vapor are as indicated on the SIMS depth profiles, Figure 4.

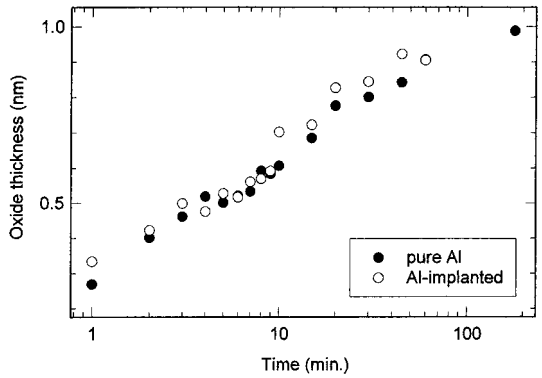

Figure 8. Oxidation of self-implanted aluminum.

equation developed by Strohmeier:[22]

$$d = \lambda_0 \sin(\phi) \ln\left(\frac{N_m}{N_o}\frac{\lambda_m}{\lambda_o}\frac{I_o}{I_m} + 1\right) \quad (1)$$

where ϕ is the electron takeoff angle with respect to the sample surface (35°); I_o and I_m are the XPS intensities (peak areas) of the oxidic and metallic components; λ_o and λ_m are the inelastic mean free paths of photoelectrons in the oxide overlayers and metal substrate; and N_o and N_m are the volume densities of metal atoms in the oxide and metal, respectively. Equation 1 assumes that the oxide overlayer is uniform and homogeneous. Although this is not exactly the case of any thin oxide films on metal, the general characteristics of changes in oxidation kinetics will not be affected if the same procedure is used in all calculations and useful information can still be obtained. Following the parameters given in Strohmeier's work,[22] the inelastic mean free paths for photoelectrons in aluminum oxide and aluminum metal are ~2.8 and 2.6 nm;[23] the ratio N_m/N_o, which is approximately equal to the atomic density ratio between the aluminum metal and the oxide γ-Al_2O_3, is estimated to be ~1.3−1.5;[24] the value of 1.5 was used in all calculations of this work. Substituting the above values into eq 1 leads to the following simplified expression:

$$d\,(\text{nm}) = 1.6 \ln\left(1.4\frac{I_o}{I_m} + 1\right) \quad (2)$$

Figures 5, 6, and 7 represent the oxide thickness as a function of exposure time for the oxidation of Fe-, Mg-, and Si-implanted aluminum, calculated using measured I_o/I_m ratios and eq 2; for comparison, the oxidation kinetics of pure aluminum are also presented.[15] These oxidation kinetics show the same trend as a function of exposure time but different behavior is found for dependence of implant doses between implanted elements. From Figure 5, it is evident that the oxide film thickness increases linearly with the logarithm of exposure time and there is no difference in oxidation kinetics between pure and Fe-implanted aluminum. By contrast, the oxidation rate of Mg-implanted aluminum shown in Figure 6 decreases with increasing surface concentration of Mg implanted until the oxide thickness has reached ~0.55 nm; after this the oxidation rate starts to increase. Finally, Figure 7 represents the effect of Si implantation on oxidation kinetics of the aluminum. In contrast to the effect of the Mg implantation, increasing the amount of implanted Si on aluminum surfaces causes an *increase* in oxidation rate.

Generally, the observed difference in oxidation rate of aluminum with added Fe, Mg and Si may result mainly from the presence of these additional elements in the oxide layers (i.e., chemical effects of implanted elements). However, in the case where the implantation technique is used, the side effects of beam interaction with the sample surfaces, such as the induced surface defects can significantly affect on oxidation kinetics. In fact, significant modifications in oxidation kinetics due to ion bombardment, with varying doses and energy, has been found for studies on Mg[25] and Al[15] conducted in this laboratory. In order to examine the effects of surface damage created by the ion beam during implantation, a series of "self-implanted" aluminum samples were prepared using the same ion beam energy 40 keV and an implant dose of 1.21×10^{13} ions·cm^{-2}. Then the oxidation kinetics was measured in the same conditions used for the other implants. The experimental results presented in Figure 8 show that there is no difference in oxidation kinetics between pure and Al-implanted aluminum. This suggests, therefore, that the surface damage due to ion beam

interaction during implantation had a negligible effect on the oxidation rate of implanted aluminum. Moreover, a supporting argument to the above conclusion can be drawn from the opposing tendency of changes in the oxidation kinetics of Mg- and Si-implanted aluminum as a function of implant dose. As the implant dose increases, a proportional concentration of defects is created in the near-surface region. As a result, any effect caused by surface disorder should be identical for both implanted Mg and Si. It must be noted that an additional number of surface defects were also introduced by Ar^+ ion bombardment for surface cleaning at the beginning of each exposure. According to the TRIM calculations (for Ar^+ ions with incident energy of 3 keV, incident angle of 60° with respect to the surface normal and Al substrate), the concentration of surface defects created by Ar^+ ion bombardment at the near-surface region is as much as twice that created by ion implantation. Hence, by maintaining the same constant cleaning procedure, all exposure experiments were carried out on surfaces prepared with the same degree of surface disorder. Consequently, the observed modification in oxidation kinetics of implanted aluminum can be related only to the presence of implanted elements in the thin oxide overlayer.

As stated in the Introduction, the presence of an additional impurity may change the transport properties in an oxide by modification of its defect structure. However, it is rather a complicated effect, which depends not only on the defect types existing in the oxide but also is affected by factors such as defect−defect interaction, relative concentrations of defects and impurity, and the crystalline microstructures of the oxide. To the best of our knowledge, there have been no fundamental investigations or data on the defect structure of thin aluminum oxide films. On the other hand, after the first few oxide layers formed, the further growth of the oxide requires transport of matter through the oxide; this, in turn, needs a certain concentration of defects to enable the diffusion of ions within the oxide structure. While the types of defects in the oxide structure define the mechanism and the direction of the transport process, their concentration determines the rate of further oxidation.

In the case of the aluminum oxide, after the fast growth up to ~2 nm a slow oxide thickening followed, best described by inverse logarithmic kinetics;[14] this could indicate an extremely low defect concentration in the first oxide layers. That, in turn, may explain the very thin layer of native aluminum oxide, with thickness not exceeding 3 nm even after long exposure times in the atmosphere.[14] On the other hand, the logarithmic kinetics of oxidation may be as a result of various determining process, which are used to be classified into one of two groups: the surface reactions and the matter transport within oxide layer.[26] Grimley and Trapnell[27] have shown that, for very thin oxide films, the rate of oxidation can be controlled by the rate of formation of vacant cation sites at the oxide/gas interface, which leads to logarithmic oxidation kinetics. In aluminum oxide, there are four possible types of ionic defects; using the notation system proposed by Kröger and Vink,[28] these defects are as follows: two vacancies V_{Al},V_O and two interstitials Al_i and O_i. As shown below, only the metal vacancies, V_{Al}, can be applied to explain fully our results of oxidation kinetics of aluminum with implanted elements. This is also in agreement with our previous results,[15] which showed that the oxidation kinetics of pure aluminum is pressure dependent and the formation of metal vacancies at the oxide film/gas interface is the determining process in the oxide growth. In an amorphous network of the aluminum oxide, similar to the crystalline structure, the metal vacancy can be a vacant position of the aluminum atom. However, the effective charge of the vacancy in an amorphous network may be lower compared with the same one in a crystalline network. This could be due to distortion in bond lengths, which facilitates the re-forming of the dangling bonds left in the area surrounding the vacancy. As such, the motion of the metal vacancy is more difficult compared with the same situation in the crystalline structure. Assuming the "ideal" amorphous network of an aluminum oxide is stoichiometric, the metal vacancy can be formed at the oxide film/gas interface according to the following reaction:

$$\frac{3}{2}O_2(g) \rightleftharpoons 2V_{Al} + 3O_O \tag{3}$$

In writing eq 3 and the further defect reactions, the following conservation rules are applied: mass conservation between two reaction sides, conservation of the stoichiometric ratio of lattice positions, and the charge neutrality in each reaction side. The built-in processes of Mg and Si elements from aluminum substrate into aluminum oxide overlayer at the metal/oxide film interface are

$$3SiO_2 \rightleftharpoons 3Si_{Al}^{\bullet} + 6O_O + V_{Al}^{'''} \tag{4}$$

$$3MgO \rightleftharpoons 3Mg_{Al}^{'} + 3O_O - V_{Al}^{'''} \tag{5}$$

reactions 4 and 5 explain well our experimental results on oxidation kinetics of Si- and Mg-implanted aluminum. As might be expected, Si and Mg introduced in the aluminum oxide will play contrary roles because of their opposite effective charges in the lattice position of aluminum: $Si_{Al}^{\bullet}$ (effective charge of +1) and $Mg_{Al}^{'}$ (effective charge of −1). According to these equations, every 3 atoms of Si or Mg introduced into aluminum oxide respectively cause a formation or consumption of a metal vacancy. Thus introducing Si or Mg element from the aluminum substrate into the oxide overlayer will result in either an increase or a reduction of the number of defects in the oxide layers, and therefore, the relevant changes in oxidation kinetics are observed. It should be noted that if the other type of defect, $Al_i^{\bullet\bullet\bullet}$ or $V_O^{\bullet\bullet\bullet}$, were the major defect in aluminum oxide, it would result in an opposite effect to that of $V_{Al}^{'''}$; i.e., the defect concentration would decrease with increasing Si and increase with increasing Mg introduction. The presence of an oxygen interstitial, $O_i^{''}$, in the network of aluminum oxide is rather unlikely because of high reactivity of aluminum with oxygen.

In the case of implanted Mg, after the oxide layers have reached a thickness of ~0.55 nm a rapid increase in oxidation rate was observed (Figure 6), which appears to be stronger as the Mg implant dose increases. From the above discussion, this inversion in oxidation rate can result from an increase of the defect concentration in the oxide as it grows further. In our defect structure suggested above, one of the possible mechanisms which may give rise to such a change in the number of metal vacancies is a transition involving an element occupying the cation lattice positions into interstitial positions. Compared with the more stable spinel phase $AlMg_2O_4$, where the Mg atoms are in tetrahedral coordination of oxygen atoms, the transition of Mg atoms from Al lattice sites to interstitials in the oxide film, as described below by eq 6, is quite possible:

$$Mg_{Al}^{\bullet} \rightleftharpoons Mg_i^{\bullet\bullet} + V_{Al}^{'''} \tag{6}$$

In this transition a vacancy left behind will contribute to an

increase in the number of defects; this explains the observed stronger increase in oxidation rate at higher Mg implant doses.

The effect of the presence of Fe element in the aluminum oxide is a bit more complex because of its two possible different ionization degrees, i.e., Fe^{2+} and Fe^{3+}, which can have the effective charge of -1 and 0 in the aluminum lattice position of the oxide network. Similarly, the incorporation of Fe atoms from aluminum substrate into the aluminum oxide overlayer can be described by one of the following defect reactions at metal/oxide film interface:

$$Fe_2O_3 \rightleftharpoons 2Fe_{Al}^{0} + 3O_O \qquad (Fe\ as\ Fe^{3+}) \qquad (7)$$

$$3FeO \rightleftharpoons 3Fe_{Al}^{'} + 3O_O - V_{Al}^{'''} \qquad (Fe\ as\ Fe^{2+}) \qquad (8)$$

From the literature, the diffusion of iron in the thin amorphous aluminum oxide has been confirmed by Nakanishi et al.[29] in an investigation on adhesion of thin aluminum oxide films deposited on an iron surface using the AES technique. Equations 7 and 8 represent two possible effects of iron present in an aluminum oxide, as Fe^{3+} and Fe^{2+} substituted in the aluminum lattice position, respectively. From eq 7, there would be no change in the defect structure of the aluminum oxide, if iron were present as Fe^{3+}. As a result, the iron implant will have no influence on oxidation kinetics of aluminum. Instead, if Fe^{2+} is found in the aluminum lattice position of the aluminum oxide, it would affect its defect structure just as the presence of magnesium atom (eqs 8 and 5). As observed above, the lowest surface Mg concentration that allows one to detect a change in oxidation kinetics is ~40 ppm (Figure 6). Keeping in mind the upper limit of Fe solubility in Al (i.e., ~250 ppm[30]), the dose of Fe used to give a near-surface concentration of ~80 ppm seems to be sufficient to confirm any effect that may result from the presence of an iron implant. Our results represented in Figure 5 show no difference in oxidation kinetics between pure and Fe-implanted aluminum. This suggests that the Fe^{3+} ions replacing aluminum ions in oxide lattice positions may totally be immersed in the oxide network and show no effective charge.

4. Conclusions

The effects of implanted Mg, Si, and Fe on the interaction of water vapor with aluminum surfaces have been investigated by the XPS technique. The oxidation kinetics of implanted aluminum show that adding Mg or Si results, respectively, in a lowered or an enhanced oxidation rate. In the case of the Mg implant, an increase in oxidation rate was observed after the thin oxide films reached a thickness of ~0.55 nm; a higher Mg dose caused more rapid growth. This is likely due to the change of Mg activity in the aluminum oxide related with the formation of a new phase, e.g., a nucleation of a spinel $AlMg_2O_4$. The oxidation kinetics of the aluminum appears to be unaffected by the presence of implanted iron. This suggests that in the aluminum oxide the implanted Fe may be substituted into aluminum positions with no net vacancies created. Finally, the effects of implanted Mg, Si, and Fe on the oxidation kinetics of aluminum can be interpreted on the basis of a defect model in which the metal vacancies are the predominant point defects in a thin aluminum oxide films. As a result, the growth of an oxide on pure aluminum surfaces in UHV conditions appears to be governed by the outward diffusion of cations from the metal substrate to the oxide film/gas interface.

Acknowledgment. The authors thank Alcan International Ltd. for supplying the aluminum samples used in this study, Prof. Andrzej Stokłosa and Dr. Tadeusz Bąk for many invaluable discussions.

References and Notes

(1) Kröger, F. A. *The Chemistry of Imperfect Crystals*, 2nd ed.; North-Holland: New York, 1974; Vol. 2.
(2) Doherty, P. F.; Davis, R. S. *J. Appl. Phys.* **1967**, *34*, 619.
(3) Beck, A. F.; Heine, M. A.; Caule, E. J.; Pryor, M. J. *Corros. Sci.* **1967**, *7*, 1.
(4) Eldridge, J. I.; Hussey, R. J.; Mitchell, D. F.; Graham, M. J. *Oxid. Met.* **1988**, *30*, 301.
(5) Lippens, B. C.; de Boer, J. H. *Acta Crystallogr.* **1964**, *17*, 1312.
(6) Alwitt, R. S. The Aluminum-Water System. In *Oxide and Oxide Films;* Diggle, J. W., Vijh, A. K., Eds.; Marcel Dekker: New York, 1976; Vol. 4, pp 169−254.
(7) Batra, I. P.; Kleinman, L. *J. Electron Spectrosc. Relat. Phenom.* **1984**, *33*, 175; see also references therein.
(8) Fuggle, J. C.; Watson, L. M.; Fabian, D. J.; Affrossman, S. *Surf. Sci.* **1975**, *49*, 61.
(9) Szalkowski, F. J. *J. Chem. Phys.* **1982**, *77*, 5224.
(10) Crowell, I. E.; Chen, J. G.; Hercules, D. M.; Yates, J. T., Jr. *J. Chem. Phys.* **1987**, *86*, 5804.
(11) Olefjord, I.; Mathieu, H. J.; Marcus, P. *Surf. Interface Anal.* **1990**, *15*, 681.
(12) Bushby, S. J.; Callen, B. W.; Griffiths, K.; Esposto, F. J.; Timsit, R. S.; Norton, P. R. *Surf. Sci. Lett.* **1993**, *298*, L181.
(13) Olefjord, I.; Nylund, A. *Surf. Interface Anal.* **1994**, *21*, 290.
(14) Do, T.; Splinter, S. J.; Chen, C.; McIntyre, N. S. *Surf. Sci.* **1997**, *387*, 192.
(15) Do, T.; McIntyre, N. S., manuscript in preparation.
(16) Ziegler, J. F.; Biersack, J. P.; Littmark, U. *The Stopping and Range of Ions in Solids;* Pergamon Press: New York, 1985.
(17) Ziegler, J. F. Ion Implantation Physics. In *Handbook of Ion Implantation Technology;* Ziegler, J. F., Ed.; North-Holland: New York, 1992; pp 1−68.
(18) Shirley, D. A. *Phys. Rev. B* **1972**, *5*, 4709.
(19) Ramamurthy, S.; Walzak, T. L.; Lu, S. F.; Lipson, T. C.; McIntyre, N. S. *Surf. Interface Anal.* **1991**, *17*, 834.
(20) McIntyre, N. S.; Davidson, R. D.; Weisener, C. G.; Taylor, K. R.; Gonzalez, F. C.; Rasile, E. M.; Brennenstuhl, A. M. *Surf. Interface Anal.* **1991**, *18*, 601.
(21) Lu, S. F.; Mount, G. R.; McIntyre, N. S.; Fenster, A. *Surf. Interface Anal.* **1994**, *21*, 177.
(22) Strohmeier, B. R. *Surf. Interface Anal.* **1990**, *15*, 51.
(23) Tanuma, S.; Powell, C. J.; Penn, D. R. *Surf. Interface Anal.* **1988**, *11*, 577.
(24) Lide, D. R., Ed. *CRC Handbook of Chemistry and Physics*, 75th ed.; CRC Press: Cleveland OH, 1994/95.
(25) Splinter, S. J.; McIntyre, N. S.; Palumbo, G. *Surf. Sci.* **1994**, *302*, 93.
(26) Kofstad, P. *High-Temperature Corrosion*; Elsevier: New York, 1988; p 149.
(27) Grimley, T. B.; Trapnell, E. M. W. *Proc. R. Soc. London, Ser. A* **1956**, *234*, 405.
(28) Kröger, F. A.; Vink, H. J. *Solid State Phys.* **1956**, *3*, 307.
(29) Nakanishi, M.; Okuya, H.; Nakajima, K. *J. Tribology* **1993**, *115*, 615.
(30) Davis, J. R., Ed. *Aluminum and Aluminum Alloys*; ASM International: Materials Park, OH, 1993.